



3

4

5

7

9

10

11

12

13

14

15

16

17

18

19

20 21

22

23

24

26

27

28

29

30

31

33

34

35

36

37

38

40

41

42

43

44

Article

Development of a vascularized human skin equivalent with hypodermis for photoaging studies

Martina M. Sanchez 1, Thamidul Islam Tonmoy 1, B. Hyle Park 1 and Joshua T. Morgan 1,*

- ¹ Department of Bioengineering, University of California, Riverside, Riverside, CA 92521
- * Correspondence: jmorgan@engr.ucr.edu

Abstract: Photoaging is an important extrinsic aging factor leading to altered skin morphology and reduced function. Prior work has revealed a connection between photoaging and loss of subcutaneous fat. Currently, primary models for studying this are *in vivo* (human samples or animal models) or *in vitro* models, including human skin equivalents (HSEs). *In vivo* models are limited by accessibility and cost, while HSEs typically do not include a subcutaneous adipose component. To address this, we developed an "adipose-vascular" HSE (AVHSE) culture method, which includes both hypodermal adipose and vascular cells. Further, we tested AVHSE as a potential model for hypodermal adipose aging via exposure to 0.45 ± 0.15 mW/cm² 385 nm light (UVA). One week of 2 hour daily UVA exposure had limited impact on epidermal and vascular components of the AVHSE, but significantly reduced adiposity by approximately 50%. Overall, we have developed a novel method for generating HSE that include vascular and adipose components and demonstrated potential as an aging model using photoaging as an example.

Keywords: HSE; human skin equivalent; tissue engineering; self-assembly; scaffold; aging; photoaging

1. Introduction

Human skin provides essential physical protection, immune barrier function, and thermal regulation [1]. As humans age, there is a decline of skin function, including loss of barrier function and healing capacity [2]. This correlates with structural changes including decreased vasculature, decreased dermal elasticity and collagen organization, stiffening, lower hydration, reduced dermal and hypodermal (or subcutaneous fat) volumes [3-17]. These detrimental effects of natural aging are compounded by extrinsic aging factors including ultraviolet A (UVA; 320–400 nm) [18] photoaging that occurs with sun exposure [2,19–21]. With normal aging, the skin is smooth with fine wrinkles and has decreasing elasticity. With photoaging skin is coarse, rough, even lower elasticity, and has changes in pigmentation [9,17]. Particularly, UVA sun exposure mainly damages by generation of reactive oxygen species [18,22]; the primary effects are in the dermis and hypodermis; with the epidermis being primarily damaged by UVB. Further, UVA exposure to human skin has demonstrated decreased expression of subcutaneous adipokines such as adiponectin [23-25]. These effects are harmful since adipokines have been found to benefit wound healing and anti-inflammatory skin properties; the hypodermis as a whole contributes to thermal regulation, skin elasticity and regeneration [26,27]. UVA exposure additionally degrades the dermal matrix through decreases in procollagen synthesis and increases in MMP-1, -3, and -9 expression [23-25]. Photoaged skin has also exhibited reduced dermal vasculature and dermal connective tissue breakdown and disorganization in human explant cultures [3,18,25,28–30].

Human Skin Equivalents (HSEs) are *in vitro* tissue models that have been previously used for studies on photoaging, wound healing, skin development, alopecia, disease, stem

Citation: To be added by editorial staff during production.

Academic Editor: Firstname Lastname

Received: date Accepted: date Published: date

Publisher's Note: MDPI stays neutral with regard to jurisdictional claims in published maps and institutional affiliations.



Copyright: © 2022 by the authors. Submitted for possible open access publication under the terms and conditions of the Creative Commons Attribution (CC BY) license (https://creativecommons.org/license s/by/4.0/).

46

47

48

49

50

51

52

53

54

55

56

57

59

60

61

62

63

64

65

66

67

68

69

70

71

72

73

74

75

76

77

78

79

80

81

83

85

86

87

88

90

91

92

93

94

cell renewal, and toxicology screening research [31–50]. The models rely on self-assembly of skin components within an appropriate matrix. Traditionally-used animal models such as rabbits, pigs, mice, and rats have different physiology than humans, for example in wound healing [31,51]. These examples add to longstanding recognition of the limitations inherent to animal models [52] and bolster recent consideration of reduction strategies [53,54]. While HSEs present with limitations of their own, they are increasingly demonstrated as useful models for human skin [34–38].

Although HSE research has been well developed to recreate the dermal and epidermal layers using fibroblasts and keratinocytes, novel co-culture systems are needed to recapitulate human anatomy more closely [55] and mimic trophic factor exchange of different cell populations *in vivo* [40,55–58]. Building on our previously published protocol generating vascularized HSE (VHSE) [59,60], here we demonstrate inclusion of a hypodermis, which we term adipose and vascular human skin equivalent (AVHSE), and demonstrate suitability for UVA photoaging studies. Multi-cellular skin models similar to this AVHSE have been previously explored but with fewer cell types, much shorter culture lengths, and little to no volumetric characterization [61–64]. UV photoaging has been previously investigated with *in vitro* skin models of the epidermis [50], keratinocytes in 2D [65], dermal fibroblasts in 2D [66,67], and adipose components in 2D [24,26]. This work combines photoaging studies with comprehensive *in vitro* skin models and allows for volumetric quantification of epidermal, dermal, and hypodermal components through volumetric imaging (confocal and optical coherence tomography). Further, the effects of photoaging on adipokine and inflammatory cytokines have been quantified using ELISA.

2. Materials and Methods

2.1. Cell Culture

AVHSE cultures were created using a modified form of our prior VHSE protocol [59,60]. Briefly, N/TERT1 human keratinocytes (hTERT immortalized; gift of Dr. Jim Rheinwald and Dr. Ellen H. van den Bogaard [31,68]), HMEC1 human microvascular endothelial cells (SV40 immortalized; ATCC, Manassas, VA; #CRL-3243) [69], and primary adult human dermal fibroblasts (HDFa; ATCC #PCS-201-012) were used as previously described, and ASC52telo adipose derived mesenchymal stem cells (hTERT immortalized; ATCC #SCRC-4000) [70] were included for the hypodermis. All cell lines were routinely cultured at 37 °C and 5% CO2; all media blends given in supplemental Table 1. N/TERT1 cells have been shown to maintain normal epidermal behavior in previous organotypic skin cultures [31,35,68]. N/TERT1 cells (passages: 8,10,16,19) were grown up in a modified K-SFM media blend including K-SFM base, 0.2 ng/mL endocrine growth factor (EGF), 25 µg/mL bovine pituitary extract, 0.3 mM CaCl₂, and 1% penicillin/streptomycin (PCN/STREP). N/TERT1 were routinely passaged once 30% confluence was met to prevent undesired differentiation in 2D cultures [68]. HMEC1 cells were grown up in MCDB1 base media with 10 mM L-glutamine, 1 μg/mL hydrocortisone, 10 ng/mL EGF, 10% FBS, and 1% PCN/STREP. HMEC1 cells at passages 9 and 11 were used. HDFa were originally expanded in fibroblast basal media supplemented with fibroblast growth kit per manufacturer instructions. For short term expansion immediately prior to AVHSE cultures, HDFa cells (all passage 4) were grown up in DMEM (4.5 g/L glucose) supplemented with 5% FBS and 1% FBS. ASC52telo were used to generate the adipose component of the skin construct. Cells were originally expanded in mesenchymal stem cell basal media (ATCC #PCS-500-030) with added supplements from a mesenchymal stem cell growth kit (ATCC #PCS-500-040) and G418 at 0.2 mg/mL; this was used as the 2D culture media until adipogenesis induction. Adipogenesis media [71,72] (recipe given in Table 1) was administered once ASC52telo plates were ~90% confluent (ASC52telo passages: 6, 8, 10 were used for AVHSEs).

Table 1. Media used for 2D and 3D culture.

Cell Line or Culture Period	Recipe	Notes	Corresponding Timepoint
N/TERT 1	K-SFM base media 1% P/S Bovine Pituitary Extract (BPE) [25 µg/mL] Epidermal Growth Factor (EGF) [0.2 ng/mL] CaCl ₂ [0.3 mM]	Media recipe based off of these references [31,68]. BPE and EGF are from the K-SFM supplement kit.	Maintenance culture
HMEC1	MCDB131 base media 10% FBS 1% P/S L-Glutamine [10 mM] Epidermal Growth Factor (EGF) [10 ng/mL] Hydrocortisone [10 ug/mL]	Media recipe as recommended by manufacturer.	Maintenance culture
Human Dermal Fibroblasts	DMEM HG base 5% FBS 1% P/S	Media used for short term expansion in 2D. For longer expansion, use the manufacturer recommendation.	Maintenance culture
ASC52telo	Mesenchymal Stem Cell Basal Medium 2% MSC supplement L-Alanyl-L-Glutamine [2.4 mM] G418 [0.2 mg/mL]	MSC Basal Medium is from ATCC (ATCC PCS-500-030); To make the complete medium the MSC growth kit (ATCC PCS-500-040) is added. MSC supplement from the growth kit contains: 2% FBS, 5 ng/mL rhFGF basic, 5 ng/mL rhFGF acidic, 5 ng/mL rhEGF.	Maintenance culture
Adipogenesis Differentiation media	DMEM/HAM's F12 base media 3% FBS 3-isobutyl-1-methyl-xanthane (IBMX) [250 µM] Indomethacin [10 µg/mL; 28 µM] Insulin [5 µg/mL]	Media recipe is based on prior work [71,72]. IBMX, Insulin, and Dexamethasone stocks stored at - 20 °C. Indomethacin,	3 weeks prior to dermal seeding. 1 week for 2D culture and 2

	Dexamethasone [1 μM]	D-pantothenate, and	weeks for 3D	
	D-pantothenate [34 μM]	Biotin stocks stored at	culture.	
	Biotin [66 μM]	4 °C.		
		This media blend is		
		not used by itself for		
		AVHSE culture, but it		
	DMEM/IIAM/a E10 lana ana dia	is used to make		
Adipocyte	DMEM/HAM's F12 base media	dermal submersion	Used indirectly	
Maintenance	Insulin [5 μg/mL]	media. Adipocyte	for Dermal	
Media	Dexamethasone [1 μM]	maintenance media is	Submersion	
(serum free)	D-pantothenate [34 μM]	adipogenesis	media.	
	Biotin [66 uM]	differentiation media		
		without IBMX or		
		Indomethacin (a		
		PPARγ agonist) [72]		
		Dermal submersion		
	1:1 Serum Free Adipocyte	media is half		
	Maintenance media and serum	adipocyte		
	free HMEC1 media	maintenance media	During week 4	
Dermal		and half HMEC1	of culture:	
Submersion	Aliquot supplement: 3% FBS	media with	dermal cells	
(DS)		supplement changes.	are seeded and	
	Daily supplements: L-Ascorbic	Media prepared	dermis is	
	Acid [100 µg/mL], VEGF [2	serum-free and used	maturing.	
	ng/mL]	as base for ESM and		
		AVHSE media.		
	Dermal submersion media with			
Epidermal	CaCl ₂ [1.44 mM]	Media used for	During week 4	
-		addition of N/TERT1s,	of culture:	
Seeding and maturation	Aliquot supplement: 1% FBS	shares base with DS	epidermal cells	
media (ESM)		and AVHSE media.	are seeded and	
media (ESWI)	Daily supplements: L-Ascorbic	and AVIISE media.	maturing.	
	Acid [100 μg/mL]			
		AVHSE media is	~4 weeks into	
	Dermal submersion media with	serum free. L-ascorbic	whole culture	
	CaCl ₂ [1.44 mM]	acid is important for	and through	
AVHSE media		collagen synthesis by	culture	
	Daily supplements: L-Ascorbic	fibroblasts, collagen	endpoint.	
	Acid [100 μg/mL], Selenium	stability, vessel wall	Media is used	
	(sodium selenite) [30 nM]	integrity and barrier	for ALI.	
		function [73–78].		

2.2. Collagen Isolation: Rat-Tail Collagen

Collagen Type I was isolated from rat tail tendons as described previously [79–82]. Briefly, tendons were extracted from rat tails (Pel-Freez Biologics, Rogers, AR), washed in Dulbecco's phosphate buffered saline (PBS) and soaked in acetone for 5 minutes, 70% isopropanol for 5 minutes, and then dissolved in 0.1% glacial acetic acid for at least 72 hours rocking at 4 °C. After dissolving, collagen was centrifuged at ~20,000× g for 1 hour and the supernatant was frozen at –80 °C and lyophilized for long term storage at –80 °C. When ready to use, collagen was dissolved in 0.1% glacial acetic acid to 8 mg/mL and stored at 4 °C.

2.3. Construct Fabrication Overview

Generation of AVHSE cultures includes four main steps, shown graphically in **Figure** 1: (1) adipogenesis, (2) dermal seeding and maturation, (3) epidermal seeding, and (4) air liquid interface (ALI); total duration is approximately twelve weeks: adipose differentiation (3 weeks), dermal maturation (<1 week), epidermal seeding (2–3 days), air liquid interface exposure (8–9 weeks). Collagen gel was used to create the hypodermis and dermal layer of the AVHSE constructs in 12-well culture inserts (translucent PET, 3 µm pore; Greiner Bio-One, Monroe, NC; ThinCerts #665631), similar to previously used [31,35–38,42,43]. In all cases, final collagen concentration was 3 mg/mL [59].

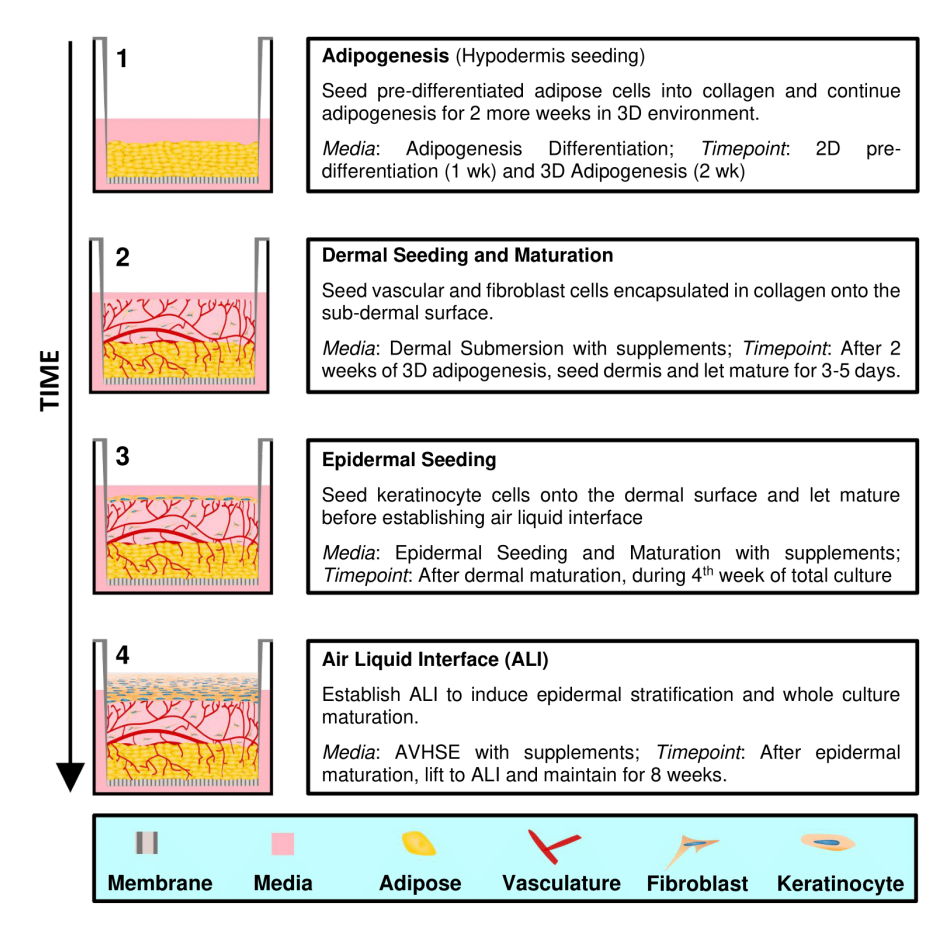


Figure 1. AVHSE generation. There are four main steps in creating an AVHSE: (1) Adipogenesis, (2) Dermal seeding and maturation, (3) Epidermal seeding, (4) Air liquid interface. Cartoons on the left show cross-sectional representations of AVHSE during each step.

2.4. Adipogenesis and Hypodermal Seeding

ASC52telo cells were grown to > 90% confluent and adipogenesis was induced for 3 weeks (media blend given in **Table 1**), split between 1 week in 2D culture and 2 weeks in

3D culture. For 3D culture, ASC52telo cells (750,000 cells/mL of collagen) were encapsulated in 125 μ L of 3 mg/mL collagen and seeded into the culture insert. After gelation, constructs were submerged with adipogenesis media (~0.5 mL and ~1 mL of media in the culture insert and well, respectively). Media was added to the insert chamber first to prevent detachment of the collagen from the membrane). Media was changed every 2–3 days until dermal seeding.

2.5. Dermal/Epidermal Seeding & Air Liquid Interface

Media was aspirated from each well and 250 µL of 3 mg/mL collagen with HMEC1 and HDFa cells (750,000 and 75,000 cells/mL of collagen, respectively) was seeded onto the hypodermis then quickly transferred to 37 °C for gelation. After gelation, constructs were submerged with dermal submersion (DS) media (Table 1) supplemented with 3% FBS, 2 ng/mL vascular endothelial growth factor (VEGF-A; Peprotech, Cranbury, NJ; #100-20) and 100 µg/mL L-ascorbic acid (L-AA; Thermo Fisher Scientific, Waltham, MA). Media was changed every 2-3 days with fresh L-AA [59,79,83]. After 3-5 days of growth in submersion, DS media was aspirated and epidermal seeding and maturation media (ESM) supplemented with 1% FBS and 100 µg/mL L-AA (1.5 mL added to each well). N/TERT1 keratinocyte cells were immediately seeded dropwise at 170,000 cells per insert (~1.13 cm² growth area) using 200 µL of their maintenance media, K-SFM. One/two days after epidermal seeding, media was changed to AVHSE media and the cultures were lifted to ALI within 8–24 h, with longer times leading to increased contraction [59]. The process to establish ALI was outlined previously [59]; typical ALI was established with ~1 mL of media. Following ALI establishment, media was changed every 2-3 days with AVHSE media and supplemented with 100 µg/mL L-AA and 30 nM selenium (sodium selenite; ThermoFisher Scientific, Waltham, MA).

2.6. Photoaging of AVHSEs

After completing 7 weeks at ALI, AVHSEs were exposed to UVA to model photoaging (PA). A UVA LED array was established by drilling a 5 mm through-hole at center of each well in the plate lid, and inserting a 385 nm/80 mcd LED (VAOL-5GUV8T4; VCC, Carlsbad, CA); 1 LED directly illuminated each insert (**Figure S1**). Four LEDs were powered in series with ~10 mA, providing a 0.45 ± 0.15 mW/cm² dose as measured by a UV sensor (UVAB Digital Light Meter, #UV513AB, General Tools & Instruments, Secaucus, NJ). LEDs were measured every 3–4 days and replaced as needed. AVHSEs were exposed to UVA for 2 hours daily for one week using an automated timer. UV dose and exposure was determined within values of prior work on human skin equivalents, cell monolayers, and mouse models [18,23,24,26,50,84,85].

2.7. ELISA (Adiponectin, IL-6, MMP-1)

AVHSE culture supernatant was collected at the end of ALI week 8 from controls and photoaged samples. Samples were centrifuged and frozen at –80 °C until use. ELISAs were performed for human Adiponectin, Interleukin-6 (IL-6), and total matrix metalloproteinase (MMP-1) according to the manufacturer's protocol (Proteintech Group, Rosemont, IL). Each sample was assayed in duplicate with standards completed for each run. For color development, tetramethylbenzidine (TMB)-substrate exposure was 20 minutes for Adiponectin and IL-6 and 15 minutes for MMP-1 at 37 °C in the dark. After stop solution was administered, color development was immediately measured at 450 nm with a correction wavelength of 630 nm using a SpectraMax M2 Multi-mode microplate reader (Molecular Devices, San Jose, CA) and corrected against a run zero standard. Four parametric logistic curves (4PLC) fits were used and values below detection limit were set to zero. Sample sizes varied for each assay due to sample availability and are as follows: Adiponectin: for each condition n = 10, r² = 0.9975; IL-6: control n = 6 and photoaged n = 8,

 r^2 = 0.9993; MMP1: control n = 7 and photoaged n = 10, r^2 = 0.9954 (9 values) and 0.91 (7 values).

2.8. Post-Culture Immunostaining and Confocal Microscopy

After culture, samples were pre-fixed in 4% paraformaldehyde for 5 minutes then fixed for 1 hour in 4% paraformaldehyde and 0.5% Triton X100 at room temperature. Samples were washed three times in PBS then stored at 4 °C until staining. For staining, culture insert membranes were removed using forceps, as described previously [59]. The staining and imaging processes were completed in four phases: epidermal, dermal vasculature, adipose, and post-clearing (**Table 2**). The nuclear marker DRAQ7 was administered during the epidermal staining phase and was used until imaging was completed. Imaging orientation of the AVHSEs were dependent on stain phase (**Table 2**). For staining, primary and secondary antibody stain solutions were made up in blocking buffer (**Table 2**). All samples were stored at 4 °C in PBS until imaging.

To image each fixed sample, custom polydimethylsiloxane (PDMS; Dow Corning, Midland, MI) molds were punched specific to each sample size and adhered to glass slides [59]. Samples were placed in the well with PBS and covered with another glass slide to preserve humidity while imaging. As AVHSE are too thick for direct confocal imaging throughout the structure without tissue clearing, each sample was imaged in both apical and basal orientations. Stains were multiplexed to laser excitations in cases of minimal overlap (e.g. epidermal and subdermal stains), and this was confirmed through the sequential staining process.

Table 2. Staining sequence, antibodies, and blocking buffer used.

Staining Sequence			
Stain/Imaging Phase	Staining/Processing Used	Imaging Orientation	
1. Epidermal	Cytokeratin 10, Involucrin, DRAQ7	Apical	(epidermal)
2. Dermal Vasculature	Collagen IV	Basal (hypodermis)	
3. Adipose	BODIPY	Basal (h	nypodermis)
4. Post-clearing	(Methanol dehydration, methyl salicylate clearing)	Basal (hypodermis)	
	Epidermal Stai	ning	
Antibody/Stain	Information & Source	Concentration	Notes
DRAQ 7	Cell Signaling;	[1:250]	Nuclear marker
Cytokeratin 10			
Primary	Cytokeratin 10 (DE- K10) mouse IgG, supernatant. Santa Cruz; sc-52318		Suprabasal
Secondary	Goat Anti-Mouse IgG (H&L), DyLight™ 488. Thermo Scientific; 35502 (1 mg/mL)	[1:500]	epidermal marker

Involucrin			
	Involucrin rabbit		
	polyclonal IgG.		
Primary	Proteintech;		
	55328-1-AP (30 µg/150		6 6
	μL)		Stratum Corneum,
	Anti-Rabbit IgG (H&L)		terminal differentiation
	(GOAT) Antibody,		
	DyLight™ 549		marker[32]
Secondary	Conjugated.	[1:500]	
	Rockland		
	Immunochemicals;		
	611-142-002		
	Dermal Vasculature	Staining	
Collagen IV			
	Collagen IV rabbit		
Primary	polyclonalProteintech;	[1:500]	
	55131-1-AP		
	Anti-Rabbit IgG (H&L)		Vascular basement
	(GOAT) Antibody,	[1:500]	membrane
Secondary	DyLight™ 549		
Secondary	Conjugated. Rockland		
	Immunochemicals;		
	611-142-002		
	Adipose Stain	ing	
	Difluoro{2-[1-(3,5-		
	dimethyl-2H-pyrrol-2-		
	ylidene-N)ethyl]-3,5-		
BODIPY	dimethyl-1H-	[2 µM]	Mature adipocyte
	pyrrolato-N}boron;	2 1 3	marker
	dissolved in 200 proof		
	EtOH, CAS: 121207-31-		
	6; Aldrich; 790389		
	Clearing		
Methanol	CAS: 67-56-1	4 baths, 10	For sample
		min. each	dehydration.
Methyl Salicylate	CAS: 119-36-8	4 baths, 5 min.	For sample
•	DI 11 D 44	each	clearing
n.	Blocking Buffer	-	t
<i>Reagent</i> ddH2O		Amount	
			50 mL
10 >	c PBS	5	0 mL

Bovine Serum Albumin (BSA)	5 g	
Tween 20	0.5 mL	
Cold water Fish Gelatin	1 g	
Sodium Azide (10% Sodium Azide in diH2O)	5 mL (0.1 % final concentration)	
All exposure for stains and antibodies: 48 hours, stationary, 4 °C		

2.9. Tissue Clearing

After completing staining and imaging phases 1–3, constructs were cleared via methyl salicylate with methanol dehydration. Constructs were dehydrated in methanol with 4x 10 min baths then cleared in methyl salicylate with 4x 5 min baths. Constructs were stored in methyl salicylate and imaged via confocal microscopy on the same day, as detailed previously [59,60].

2.10. Quantitative Epidermal Analysis

Thickness of epidermal layers were automatically detected from confocal images via thresholding differences using a custom analysis algorithm designed in MATLAB (MATLAB 2018b; Mathworks, Natick, MA), similar to prior descriptions [60]. For each sample, five confocal sub-volumes in the center of the AVHSE were used to detect thickness (total volume of 1.85 × 0.37 × 0.25-0.4 mm; imaging depths were adjusted per sample but a consistent voxel size of $0.7 \times 0.7 \times 3 \mu m$ was used). An average thickness was found for each XY position to obtain a volumetric thickness indication rather than from a single cross-sectional position or from max projection. Briefly, epidermis was localized using DRAQ7, cytokeratin 10, and involucrin stains. Noise was removed using median filters applied to each XY-plate and intensities were scaled by linear image adjustment. Background auto-fluorescence was removed using rolling ball filters on each XY plane and the epidermis was segmented using hysteresis thresholding. Gaps in the epidermal binary volume were removed via morphological closing and opening with a disk structuring element. The resulting binary volume created a computational plane from which the top and bottom difference could be calculated and metrically scaled by appropriate voxel size. Intensity comparison of the suprabasal markers, Cytokeratin 10 and Involucrin, was completed across all samples using confocal images. A maximum projection image of ten positions per sample was generated and average intensity values were calculated. For all epidermal quantification, five AVHSE replicates were used for analysis.

2.11. Quantitative Dermal/Hypodermal Analysis

Adipose thickness, volume fraction (VF), and integrated intensity quantification was completed from 10 confocal sub-volumes per each sample (a total volume of $3.7 \times 0.37 \times 0.35$ mm). VF is an estimate of the adipose within the hypodermis and dermal space. Volumetric thickness was calculated using localization of the BODIPY mature adipose marker, as described for epidermal thickness quantification. Integrated intensity of BODIPY was quantified via custom algorithms. Briefly, image sub-volumes were segmented and the resulting binary masks were used to isolate BODIPY stain from background noise and autofluorescence. The sum of raw intensity along the z-axis was calculated for each sub-volume within its binary map, then all sub-volume values were averaged as a metric of the whole sample volume. These data were gathered from images taken in the $3^{\rm rd}$ imaging phase (**Table 2**). Six AVHSE replicates were used for analysis.

Vascular quantification parameters of diameter, VF of the vasculature, and diffusion length (R_k) were determined from the average of 6 confocal sub-volumes per each sample (total volume of $2.22 \times 0.37 \times 0.35$ mm), similar to published methods [59,79,86]. Using the Collagen IV marker from cleared AVHSE structures (4^{th} imaging phase, **Table 2**), vessels were located through segmentation (using built-in MATLAB functions, custom functions,

193 194

195

196

197

198

199
a 200
a 201
a 202
t 203
r 204
s 205
a 206
d 207
a 208
c 210
d 211
c 212

219220

221

214

215

216

218

233

234

and previously published functions [87,88]) and ultimately vessel detection via an enhanced Hessian based Frangi filter [89–91]. VF was determined using the resulting volume segmentation. After locating vessels, the segmented volume was skeletonized through a fast marching algorithm [59,79,92–94]. Diameter was quantified by performing Euclidean distance transform on the vascular segmentation and collecting values along the skeleton. Additionally, Rk was defined as a "diffusion length" from the vascular fraction that encompasses 90% of the volume [79]. Rk was obtained by determining the Euclidean distance between all points in the collagen volume and the nearest point on the network. Four AVHSE replicates each were used for analysis.

2.12. Live Culture Imaging

On a limited number of cultures, optical coherence tomography (OCT) was used as a non-invasive technique to measure epidermal thickness in live samples as previously described [60]. OCT imaging was conducted with a custom built fiber-based spectral domain optical coherence tomography (SD-OCT) system centered at 1310 nm, as described previously [95]. Each sample was imaged then immediately returned to culture while maintaining sterility, requiring imaging through the well plate lid. To minimize the reflective effect of the lid, the sample arm of the OCT system was tilted at 15° , reducing reflection while maintaining adequate illumination. Imaging took ~1 hour for each sample; no loss of sample viability was observed. Settings for imaging remained consistent through culture: 1 volumes, 400 frames, and 4096 A-lines were taken per sample; resulting image size was $4096 \times 512 \times 400$ voxel ($4 \times 2 \times 4$ mm). Epidermal thickness was assessed via post-processing of the data using custom-written scripts in MATLAB (MATLAB 2018b; Mathworks, Natick, MA) which detected the top and bottom surfaces of the hyper-reflective epidermis and calculated thickness across the volume, as previously described [60].

2.13. Statistics

Pairwise comparisons of control v. photoaged samples were completed through two-tailed t-test. ANOVA followed by Tukey's HSD post-hoc test was used to test for statistically significant differences when applicable. Un-normalized data points are shown for comparison to tissue scale morphology. For statistical comparison, data were normalized to control for epidermal, vascular, and adipose quantification. Significant differences of normalized data are plotted with p < 0.05 represented by a single asterisk; p < 0.01 represented by a double asterisk.

3. Results

3.1. AVHSE Enables Tissue-Scale Studies of Skin Biology

AVHSEs and the analysis techniques presented here enable study of skin volumetrically and at the tissue scale (**Figure 2**). Through automated imaging and stitching, epidermal, dermal, and hypodermal markers can be assessed volumetrically. The automated image analysis of the three skin compartments described in the following sections was completed on biologically large volumetric areas with minimum volumes of $\sim 1 \times 0.7 \times 0.25$ mm to analyze the epidermis and up to $3.6 \times 0.37 \times 0.35$ mm to analyze the hypodermis. Importantly, the volumetric approach allows assessment of variation across the culture that is difficult with standard histological approaches that involve sectioning [60].

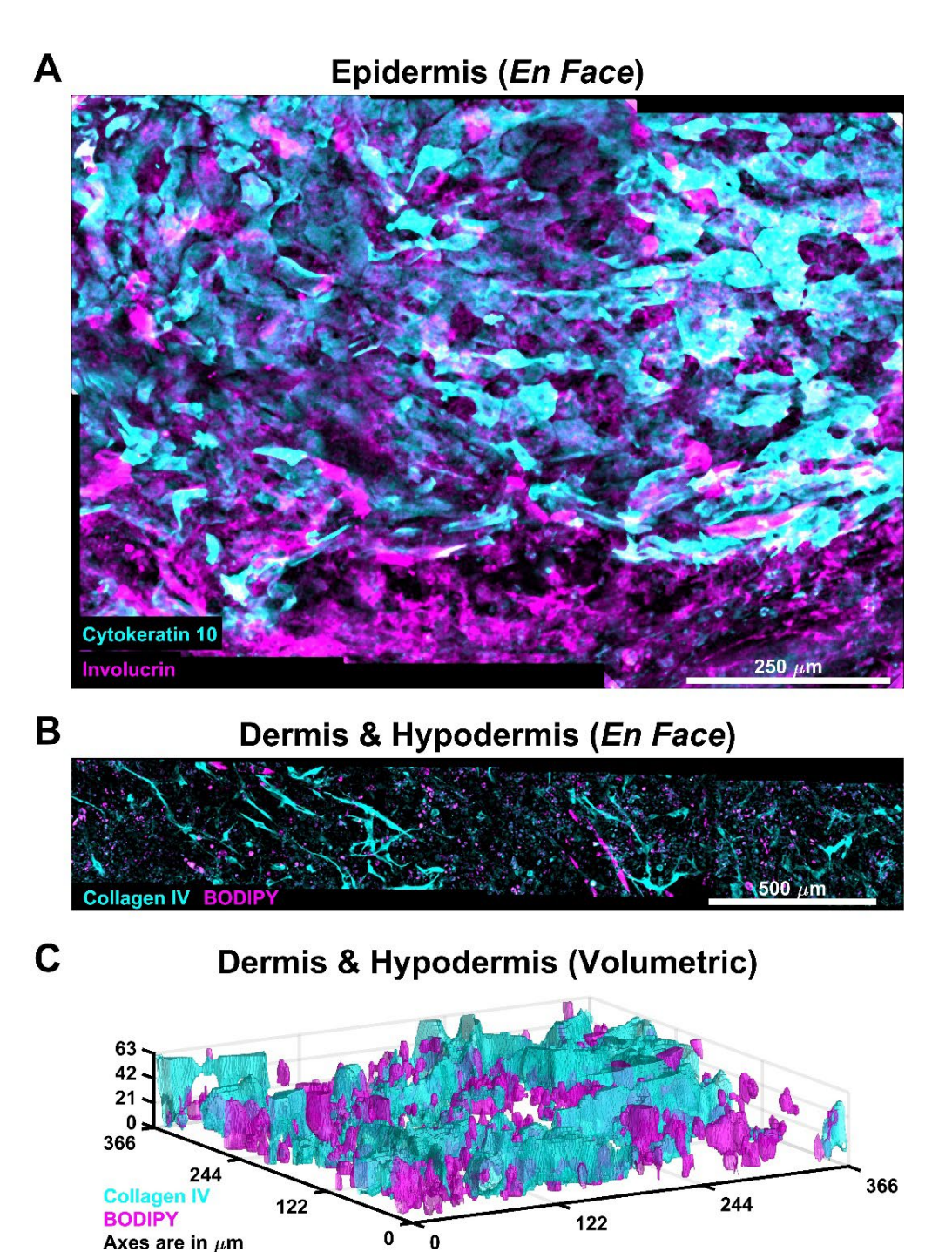


Figure 2. AVHSE allow for large-scale assessment of cultures. (**A**) Demonstration of scale of epidermal analysis. Cytokeratin 10 (cyan) is a suprabasal epidermal marker and Involucrin (magenta) is a stratum corneal marker. Image is an *en face* max projection of $\sim 0.7 \times 1 \times 0.2$ mm volume. (**B**) Adipose and vasculature morphology can be assessed at scales that span 3.6 mm (approximately half of this representative AVHSE), presented as an *en face* max projection. Collagen IV (cyan) marks the vasculature and BODIPY (magenta) marks lipid droplets secreted from mature fat cells (magenta). (**C**) Volumetric rendering of segmented Collagen IV (cyan) and BODIPY (magenta), demonstrating vascular infiltration into the hypodermis. Images were acquired preclearing and are median filtered for clarity.

3.2. UVA Photoaging Alters Adiponectin Expression

Prior studies have demonstrated decreased adipokine production during photoaging, and adipokines are mediators of the dermal photoaging mechanism [24,96].

To test if the AVHSE cultures were similarly responsive to UVA, we measured production of adiponectin using ELISA. AVHSE cultures were prepared and maintained through ALI as described in the methods. After 7 weeks of ALI, AVHSE were exposed to 7 days of UVA (2 h/day, 385 nm, 0.45 ± 0.15 mW/cm²), or left as controls. Media supernatant was collected from both photoaged and control samples after UVA exposure. Adiponectin expression was significantly reduced, in agreement with prior *in vivo* studies [24] (**Figure 3**). This was not accompanied by a general inflammatory response or increased matrix metalloproteinase-1 (MMP-1) presence, as indicated by stable IL-6 and MMP-1 expression (**Figure 3**).

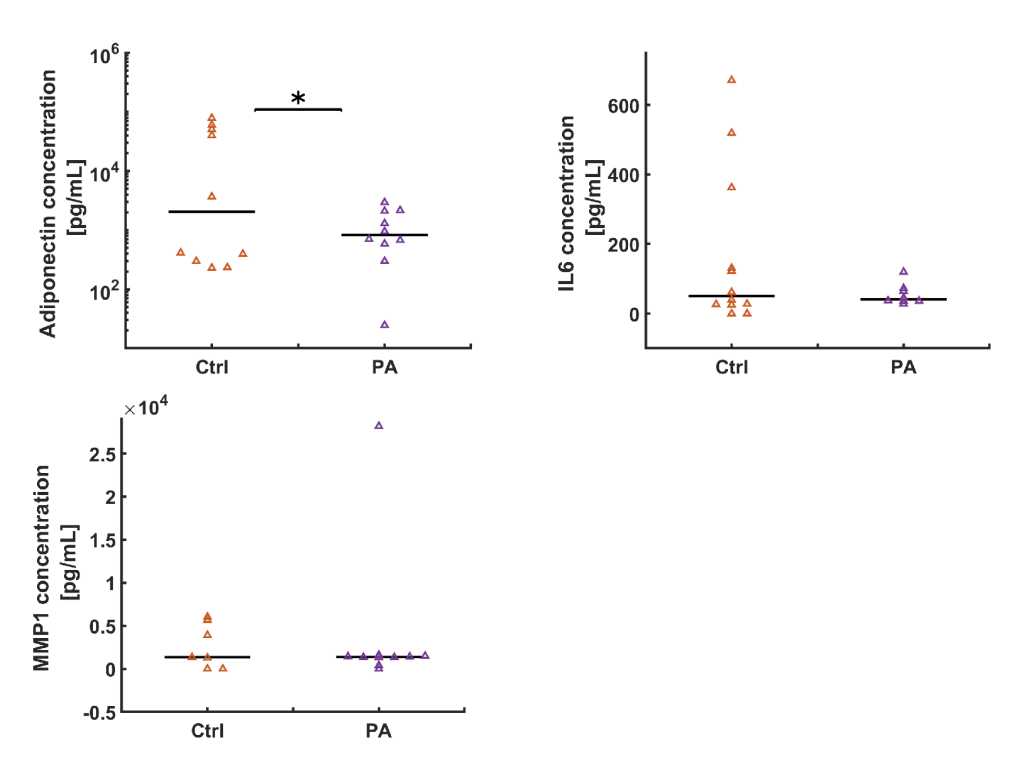


Figure 3. Cytokine evaluation from cell media was completed via ELISA. Cell media was collected after week 8 of culture. All values were corrected by a zero standard and values below detection limit were set to zero. All values were determined from four-parametric logistic curve fits. Data is shown as medians (black bars) and individual data points (triangles). Sample numbers varied for each assay due to limited culture volumes. Adiponectin: for each condition n = 10. IL-6: control n = 6 and photoaged n = 8; MMP1: control n = 7 and photoaged n = 10. A two-tailed t-test showed a significant decline in the adiponectin secreted into media after photoaging AVHSEs (p < 0.05; indicated with *).

3.3. Epidermis is Stable During UVA Photoaging

Photoaging by the UVA largely acts on the dermal and hypodermal portions of the skin rather than the epidermis, in contrast to UVB which shows epidermal toxicity [18,22]. To assess any changes in epidermal morphology, we stained suprabasal markers (involucrin and cytokeratin 10) along with the nuclear stain DRAQ7 to assess epidermal thickness. No statistically significant differences were observed in the staining intensity of involucrin and cytokeratin 10 (**Figure 4A–B**), or in the overall thickness of the epidermis (**Figure 4C**), when comparing the control and the photoaged AVHSEs. For a limited number of samples, we further assessed epidermis through OCT imaging as previously described [60]. Consistent with the confocal data we observed no gross change in epidermal morphology with photoaging. These data are consistent with the minimal *in vivo* effects of UVA on the epidermis [22].

Figure 1. Epidermal characterization and quantification. (**A**) The epidermal differentiation markers, Involucrin (magenta) and Cytokeratin 10 (cyan), localize to epidermis. Nuclei are marked with a DRAQ7 counterstain and shown in yellow. No apparent qualitative changes in the experimental groups were observed, as shown in these representative images. Scalebars are 100 μ m. (**B**) Quantification of epidermal intensities was completed from z-axis maximum projections; no indication of intensity changes were found in either epidermal stain when comparing control (Ctrl) to photoaged (PA) samples. For both control and photoaged groups n = 5. (**C**) Epidermal thickness was volumetrically quantified and no differences were indicated (n = 6 for both control and photoaged groups). Data is shown as medians (black bars) and individual data points (triangles). Images were acquired pre-clearing and are median filtered for clarity.

3.4. Dermal Vasculature is Stable during UVA Photoaging

Prior studies have shown dermal vascular damage is associated with chronic UVA exposure, as determined from sun-exposed skin biopsies from young v. aged individuals (20–80 years) [97]. As a proxy for vascular damage, we quantified overall morphology in the AVHSE. Vascular structures were identified through localization of collagen IV (**Figure 5A**). Formation of well-developed vascular networks was observed in both control and photaged samples as shown in maximum projections. Imaging for vascular quantification was performed after tissue clearing, to minimize the loss of signal deeper

335

336

337

338

339

340

341

344

345

346

347

348

349

350

351

352

353

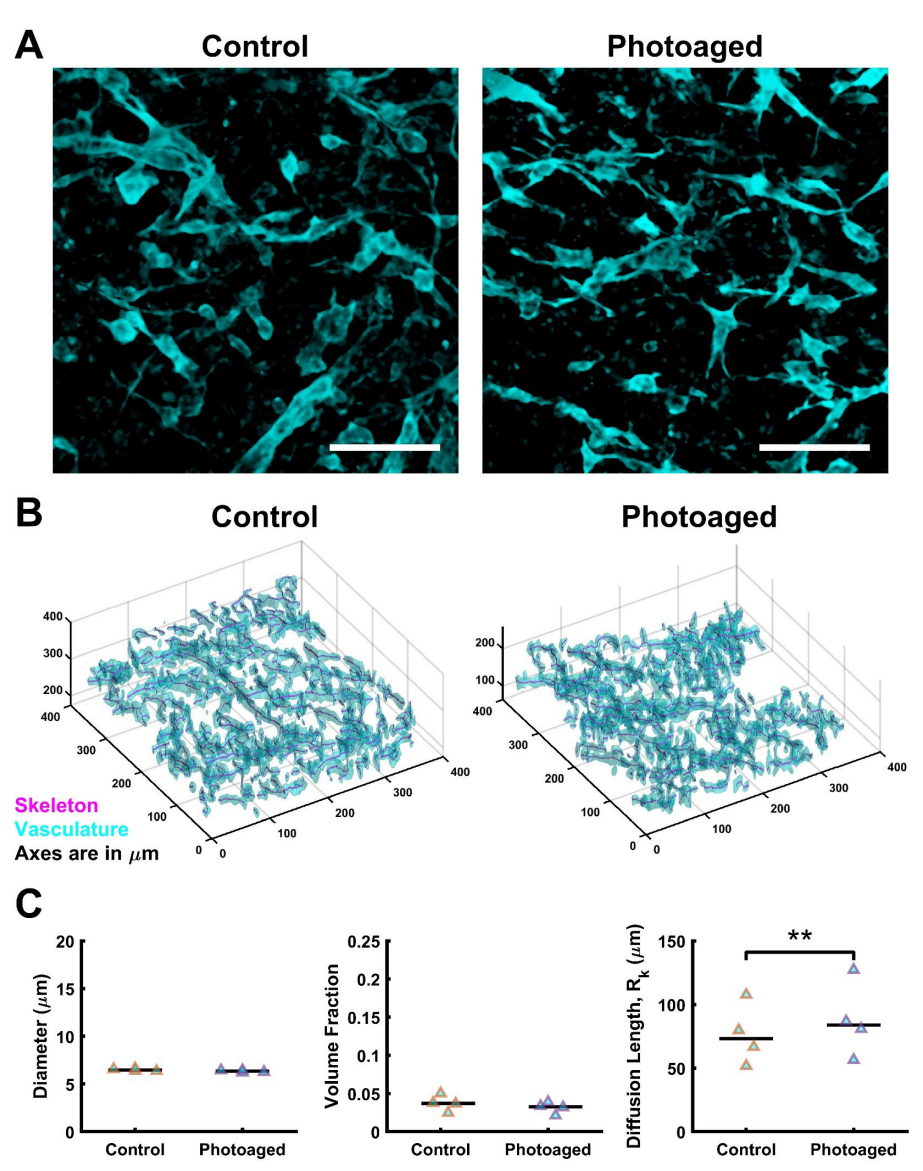


Figure 5. Vascular staining and quantification. (**A**) A comparison of maximum projections of confocal images of control v. photoaged AVHSE sub-dermis and dermis; Collagen IV marks vasculature in cyan. Scalebars are $100 \ \mu m$. (**B**) Segmentation of the vascular fraction (cyan) was completed on 6 cleared sub-volumes per sample. Skeletonization was completed using segmentation data (magenta line). Shown is a representative 3D rendering of one confocal sub-volume. (**C**) Segmentation and skeletonization of vascular networks enables quantitative assessment of the morphology (n = 4 for each condition). Vessel diameter and volume fractions remain stable when AVHSEs are photoaged and there is an increase in diffusion length for

358

359

360

361

photoaged (p < 0.01; indicated with **). Data is shown as medians (black bars) and individual data points (triangles). Images are median filtered for clarity.

3.5. Hypodermal Adiposity is Reduced with Photoaging

Prior *in vivo* studies have shown decreases in hypodermal adipose associated with UVA photoaging. To test if this was mimicked in the AVHSE model, we used confocal imaging of the lipid stain BODIPY in both controls and photoaged AVHSE. Representative images shown in **Figure 6A** show decreased staining intensity and representative volume renderings are shown in **Figure 6B**. To quantify adiposity, we utilized two morphological measures (lipid volume fraction and adipose thickness) as well as the integrated intensity of the BODIPY. Both morphological measures exhibit subtle declines, but the results are non-significant (**Figure 6C**). However, the overall stain intensity was significantly decreased (**Figure 6C**), indicating an overall loss of lipid content in the photo-aged AVHSE.

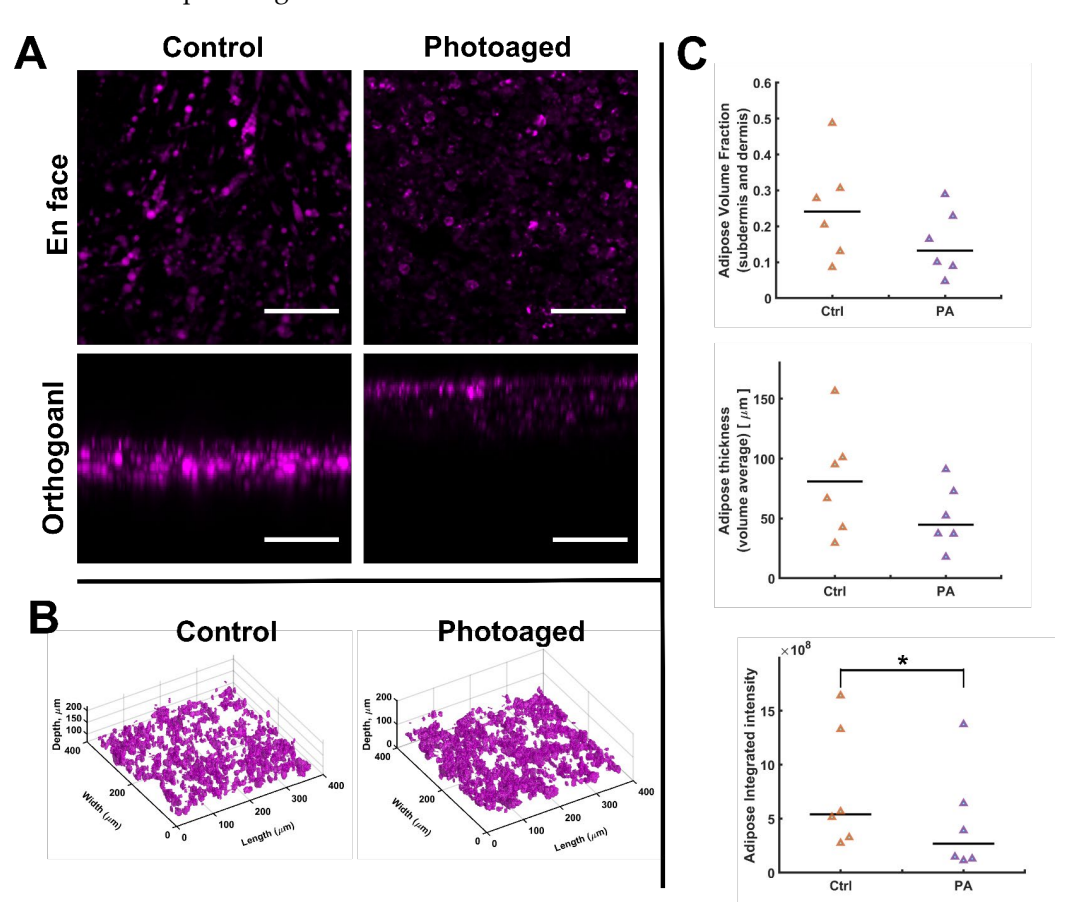


Figure 6. Adipose staining and quantification. **(A)** A comparison of confocal images of control vs. photoaged AVHSE sub-dermis; BODIPY marks lipid accumulation at mature adipocytes in magenta. Scalebars are 100 μ m. **(B)** Representative 3D rendering of adipose volume fraction for control and photoaged samples. **(C)** Top-Volume Fraction was calculated based on segmentation of the BODIPY stain as seen in B. Middle-Thickness quantification based on morphological closing of BODIPY segmentation. Bottom- Integrated Intensity of BODIPY across the volume shows a significant (p < 0.05; indicated with *) drop in photoaged samples (n = 6 for each condition). Data is shown as medians (black bars) and individual data points (triangles). Images were acquired preclearing and are median filtered for clarity.

4. Discussion

Skin provides critical barrier, insulation, and homeostatic functions in human physiology; these are known to be disrupted in aging [2,17,98]. Despite the importance, research is limited by the accessibility of physiologically relevant models, with

391

392

393

394

395

397

398

399

400

401

402

403

404

405

406

408

409

410

411

412

413

414

415

416

417

418

419

420

421

422

423

424

425

427

429

430

431

432

433

434

436

437

438

439

440

441

443

conventional culture methods lacking the structure and organization of the overall tissue [4] and conventional animal models presenting key differences from human aging physiology [31,51]. To address this, human skin equivalents (HSE) have been previously established as valuable models in the study of skin and aging [4,8,12,14,99–108]; however limitations remain. Of special relevance, loss and dysregulation of hypodermal adipose is implicated in physiological aging [98,109,110] and aging-associated diseases including lipoatrophy [111] associated with insulin-resistant diabetes mellitus [112]. This dysregulation is poorly captured in current HSE. To address this, we have developed a robust and reproducible HSE that includes adipose and vascular components (AVHSE). This methodology builds off of previous studies [62,113-116] and provides a model to study crosstalk between adipose, vascular, stromal, and epithelial components of skin in the context of aging. Further, this model is tissue-scale, stable for long culture durations (experiments described were 8 weeks, 16 week cultures have been performed using similar methods), and suitable for aging studies. Other researchers have reported that when skin models are cultured with adipose tissue, after 2 weeks of culture, there was epidermal disintegration and that 7 days is enough time at ALI to produce a fully functional skin equivalent [64]. Although we did not directly compare skin equivalents without adipose to AVHSEs here or directly compare culture timepoints, we have not observed any obvious changes in epidermal coverage compared to our previous work in vascularized human skin equivalents that do not contain a subcutaneous adipose compartment [59]. While the model is customizable to study the effects of intrinsic and extrinsic aging factors, as a test case we have demonstrated suitability for studies in UVA photoaging due to the strong literature base of both in vitro and in vivo studies available for comparison. Finally, we demonstrated the accessibility of the model for both molecular (e.g. ELISA) and morphological studies (e.g. volumetric analysis of cell organization).

A key aspect of any HSE model is a differentiated and stratified epidermis. Here, N/TERT-1 keratinocytes [68] were used to generate skin epidermis as previously completed [31,35,59]. Importantly, N/TERTs are a suitable and robust substitute to primary keratinocytes which have disadvantages including limited supply, limited in vitro passage capabilities, and donor variability [35]. HSEs generated with N/TERT keratinocytes demonstrate comparable tissue morphology, appropriate epidermal protein expression, and similar stratum corneum permeability when compared to HSEs generated with primary keratinocytes [31,35]. Similar to prior models, we demonstrate AVHSEs appropriately model the skin epidermis with correct localization of involucrin (a stratum corneum marker) and cytokeratin 10 (suprabasal early differentiation marker) [1,38] (Figure 1). Further, volumetric imaging and automated analysis allows for epidermal thickness to be robustly calculated. AVHSE present with median epidermal thicknesses within 90–100 μm, similar to values in both prior in vitro studies 100-200 μm [117] and in vivo optical coherence tomography imaging of adult skin 59 ± 6.4 to 77.5 ± 10 µm [118]. Consistent with prior in vitro and in vivo results showing UVA wavelengths predominantly impact dermal rather that epidermal layers [119,120], UVA photoaging resulted in no observable changes in epidermal thickness or expression of differentiation markers in AVHSE (Figure 3).

In the dermis and hypodermis, skin is highly vascularized with cutaneous microcirculation playing important roles in thermal regulation and immune function [98,121]. Many prior HSE models have not included a vascular component [31,34,35,43,63]; however, there is increasing recognition of its importance [1,4,40,47,48,122,123]. In the present work, we used collagen IV as a marker of the vascular basement membrane, enabling the automated segmentation and mapping of a vascular network within AVHSEs. Importantly, volumetric quantification of the vasculature was performed with imaging after tissue clearing; however, these techniques are possible with uncleared images as well with some limitations [59]. The vascular VF of AVHSEs is lower than *in vivo* dermis (~3% compared to 20.0 ± 5.0 to 40.3 ± 2.4 % measured by OCT at four positions in the arm [124]), but prior work has shown this is tunable by using different

cell seeding conditions [79]. Optimizing the VF may be more involved in the AVHSE, since the ratio of adipose and vascular cells has been shown to be important in regulating tissue morphology [113]. Thus, ratio of adipose and vascular cells would need to be optimized for new cell and collagen densities. Adipose tissue is densely vascularized [113,125,126] and the ability of adipocytes to generate lipid droplets and adipokines in the presence of endothelial cells is important to replicate the *in vivo* environment [114]. Previous work has shown that in co-culture of endothelial cells (ECs) and mature adipocytes can lead to dedifferentiation of mature adipocytes [126], but in homeostatic cultures ECs and adipocyte crosstalk is important. Through soluble factor release, ECs regulate lipolysis and lipogenesis and adipocytes regulate vasodilation and contraction [64,126]. Secretion of adipokines by adipocytes aids vascular formation and adipose tissue stability [114,126]. In prior work, Hammel & Bellas demonstrated that 1:1 is the optimal ratio for vessel network within 3D adipose [113], and we matched the 1:1 cell ratio in the present work.

Quantification of vessel diameter in the Hammel & Bellas study shows that a 1:1 ratio of adipocytes to endothelial cells gives an average vessel diameter of ~10 µm [113], our work similarly finds a median vessel diameter of ~6 µm. Importantly, these data are within the range of human cutaneous microvascular of the papillary dermis (4 to 15 μm [121]). We did not observe morphological changes of VF and diameter within the vasculature due to photoaging. While it is established that chronic UVA exposure can contribute to vascular breakdown [97,127], the duration of our studies may be too short to see this effect in diameter and VF (1 week vs lifetime UV exposure in people over 80 [3,97]). However, photoaging did induce an increase in diffusion length (R_k), in this case defined as the distance from the vasculature that covers 90% of the construct; higher values corresponds to lower vascular density. Values presented here match previous studies of vascularized collagen [79]. Rk of the vascular network for both control and photoaged samples was within the range of 51-128 μm, lower than the frequently cited 200 µm diffusion limit for supporting a cellular tissue [128]. These findings conflict with studies of acute UV exposure in skin, which show stimulation of angiogenesis [3,129]. It has been proposed that UV light exposure may improve psoriasis by normalizing disrupted capillary loops through upregulation of VEGF by keratinocytes [121]. The AVHSE model could be used to more thoroughly test the effects of UV light and other molecular mechanisms it induces in future studies.

Further, we observed vasculature colocalized with the lipid droplet BODIPY staining (Figure 2), indicating recruitment of the vascular cells to the hypodermis. Importantly, the vascular networks in prior studies and the present AVHSE are self-assembled. While there are advantages to self-assembly, especially the simplicity of the method, it is important to note the limitations. Cutaneous microcirculation *in vivo* has a particular anatomical arrangement with two horizontal plexus planes, one deep into the tissue in the subcutaneous fat region and one just under the dermal-epidermal junction [121,130]. Between these two planes are connecting vessels running along the apicobasal axis that both supply dermal tissues with nutrients and are an important part of thermoregulation [121,130]. Although the AVHSEs presented here have reasonable vascular densities they do not recapitulate this organization. While not covered in this work, future studies could incorporate layers of patterned or semi-patterned vasculature [128] to more closely match the dermal organization, depending on the needs of the researcher.

This photoaging model did demonstrate impacts to the hypodermis. Volumetric imaging of BODIPY, which stains lipid droplets [113], was used as a measure of adiposity. While small reductions in the morphological parameters (adipose thickness and lipid VF) were observed, they were not significant, suggesting there was not large-scale apoptosis or other cellular loss. However, there was a significant decrease in the intensity of BODIPY staining, indicating decreased lipid levels (**Figure 6**). This is consistent with photoaging of excised human skin showing that UV exposure decreases lipid synthesis in subcutaneous fat tissue [96]. We further collected culture supernatant and tested for the

presence of adiponectin, IL6, and MMP-1. The data collected through ELISA (**Figure 3**) show that this AVHSE model secretes both adiponectin and IL6, which are also present in native skin and both considered important adipokines [62,126,131,132]. Elevated serum adiponectin levels are linked to anti-inflammatory effects in humans [131,132] and centenarians (a model of healthy aging) have elevated levels of adiponectin [131]. Decreased adiponectin has previously been associated with photoaging in both excised human skin that was sun-exposed compared to protected skin and in protected skin that was exposed to acute UV irradiation [24]. Conversely, IL6 is a key factor in acute inflammation in skin, and has been shown to regulate subcutaneous fat function [96,133]. In prior studies of photoaging, IL6 has demonstrated an increase after UVA irradiation in monolayer fibroblast cultures [134] and excised human skin [96,133]. IL-6 is released after UV irradiation and has been linked to decreased expression of adipokine receptors and mRNA associated with lipid synthesis [24], decreases in lipid droplet accumulation [96], and enhanced biosynthesis of MMP1 [134,135]. However, after one week of photoaging we did not observe an increase in IL-6 or MMP-1 via ELISA (**Figure 3**).

The absence of changes in IL-6 and MMP-1 expression but decreases in lipid accumulation and adiponectin are not expected results but they could be due to methodology differences in UVA exposure. We determined our UVA dose and exposure based on literature values [18,23,24,26,50,84,85]. The dose used here was 0.45 ± 0.15 mW/cm² with exposure for 2 hours daily for 7 d; this converts to approximately 3.24 J/cm² per day and a total of 22.68 J/cm². Many studies do not report exposure time and/or present ambiguous timepoints. This compounded with the practice of using doses based on sample pigmentation and broad definition of UVA wavelengths may be contributing to the differences in IL-6 and MMP-1 expressions compared to prior work. While not addressed in the present study, the AVHSE culture platform is suited for future studies investigating the specific molecular mechanisms associated with altered wavelength(s), dosing, and durations.

Unexplored in this study is the mechanics of the AVHSE, and the impact of photoaging on mechanics. Acting as a defense against mechanical trauma is a key function of the skin in vivo [1], the mechanical properties that enable this are highly dependent on the structure and composition of the tissue [136]. Importantly, the collagen density in the AVHSE model is 3 mg/mL, much lower than in vivo densities [137,138]; this difference is likely accompanied by dramatically reduced mechanical strength of AVHSE compared to native skin. Increasing the collagen density to physiologically relevant levels and directly quantifying AVHSE mechanics will be an important aspect of future studies [136]. Importantly, higher collagen densities are possible through a variety of techniques, including dense collagen extractions [81] and compression of the collagen culture [41]. In addition to density, the anisotropic collagen organization of native dermis is a key factor in mechanics. It has long been understood that dermal collagen has a preferential orientation, and that the mechanical properties of skin differ parallel or perpendicular to that orientation [136,139]. In these studies, collagen alignment was not controlled and likely has no global alignment [140]; future studies that included collagen orientation could leverage a range of previously established techniques depending on the specific goals [141]. In the context of photoaging, these mechanical studies are especially relevant. Decline of collagen density is an important aspect of skin aging, correlating with skin elasticity and wound healing [4-7,11,17,142]. Further, photoaging increases the expression of MMPs and decreases collagen synthesis [23-25], resulting in fragmentation and disorganization of the dermal extracellular matrix [18]. Future studies that measure and control the mechanics of AVHSE will be important for fully characterizing the model and more closely matching the physiology of native skin.

There are additional limitations of the AVHSE model presented. Although we have presented a skin model that is closer to both anatomy and biology of human skin in comparison to past HSEs, we have not modeled skin fully through inclusion of other features of *in vivo* skin such as immune and nerve components. Including a functional

553

554

555

556

557

558

559

560

561

562

563

564

565

566

568

569

570

571

572

573

574

575

576

577

578

579

580

581

582

583

584

585

586

587

588

immune system is important in understanding autoimmune diseases, cancer, wound healing, and decline of immune function in aged skin [4,98]. Additionally, neuronal cell inclusion will allow for modeling of sensory processes necessary for grafting and modeling of skin disorders associated with nerve dysregulation [98]. Further, while the cell lines used in this study were chosen for their low cost and accessibility, primary cells or populations differentiated from induced pluripotent stem cells (iPSCs) would more closely match the physiology in vivo. While changing cell populations would likely require some adjustment to the culture system, we have previously demonstrated that cell types can be replaced with minimal changes [59]. We model epidermis, dermis, and hypodermis here, but we do not model the depth that is present in thick skin tissue. As nutrient and waste diffusion in tissues is limited to ~200 µm [128], thick tissues will likely require perfusion to maintain throughout culture. Vasculature in thicker skin has higher diameters, especially in the lower dermis and hypodermis, these can be up to 50 µm [121], and thick skin models may benefit from patterning larger vessels. Further, the AVHSE method was demonstrated with low serum requirements; while serum was used for initial growth, the cultures are maintained for weeks without serum. Serum replacements during the growth phase could potentially provide a chemically defined xeno-free culture condition in beginning culture stages for greater reproducibility and biocompatibility.

The presented AVHSE model provides unique capabilities compared to cell culture, ex vivo, and animal models. Excised human skin appropriately models penetration of dermatological products but there is limited supply and high donor variability [143]; replacing excised human skin with animal models or commercially available skin equivalents limits due to the differences such as varying penetration rates, lipid composition, lipid content, morphological appearance, and healing rates [143,144]; cost and limitations of customization are additional factors. AVHSE can be cultured using routinely available cell populations, are cost effective, and are customizable for specific research questions. Further, the model is accessible for live imaging, volumetric imaging, and molecular studies, enabling a wide range of quantitative studies. The current work focused on AVHSE as a research tool, but similar techniques could be further developed for the development of grafts. Grafting would require addressing many of the structural and biological limitations noted above, as well as modifications to address host immunity issues. Overall, we have demonstrated AVHSEs as a research platform with regards to photoaging effects, but expansions of this model could be utilized for clinical skin substitutes [73], personalized medicine, screening of chemicals/cosmetics, drug discovery, wound healing studies [73,144], and therapeutic studies [62].

Supplementary Materials: The following supporting information can be downloaded at: www.mdpi.com/xxx/s1, Figure S1: UVA Photoaging Setup.

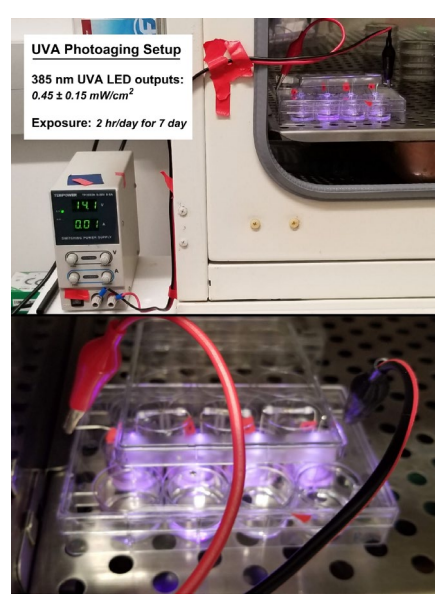


Figure S1. UVA Photoaging Setup. UVA exposure was completed by drilling out a well plate lid and inserting UVA LEDs. Each LED had an output of 0.45 ± 0.15 mW/cm². AVHSEs were exposed daily for 2 hours, for 7 days.

Author Contributions: Conceptualization, MMS and JTM; methodology, MMS, TIT, BHP, and JTM; software, MMS and JTM; formal analysis, MMS; investigation, MMS and TIT; resources, BHP and JTM; writing—original draft preparation, MMS; writing—review and editing, MMS, TIT, BHP, and JTM; visualization, MMS and JTM; supervision, BHP and JTM; funding acquisition, JTM. All authors have read and agreed to the published version of the manuscript.

Funding: This work was supported in part by the American Heart Association (19IPLOI34760636). This material is based upon work supported by the National Science Foundation under Grant No. CAREER 2046093.

Data Availability Statement: The data that support the findings of this study are available from the corresponding author, JTM, upon reasonable request.

Acknowledgments: The authors thank Dr. Jim Rheinwald and Dr. Ellen H. van den Bogaard for their generous gift of N/TERT cell lines.

Conflicts of Interest: The authors declare no conflict of interest. The funders had no role in the design of the study; in the collection, analyses, or interpretation of data; in the writing of the manuscript; or in the decision to publish the results.

References

- 1. Mathes SH, Ruffner H, Graf-Hausner U. The use of skin models in drug development. Advanced Drug Delivery Reviews. 2014 Apr 20;69–70:81–102.
- Fenske NA, Lober CW. Structural and functional changes of normal aging skin. Journal of the American Academy of Dermatology. 1986 Oct 1;15(4, Part 1):571–85.
- 3. CHUNG JH, EUN HC. Angiogenesis in skin aging and photoaging. The Journal of Dermatology. 2007 Sep 613 1;34(9):593–600.
- 4. Ali N, Hosseini M, Vainio S, Taieb A, Cario-André M, Rezvani HR. Skin equivalents: skin from reconstructions as models to study skin development and diseases. British Journal of Dermatology. 2015;173(2):391–403.

5.	Farage MA, Miller KW, Zouboulis CC, Piérard GE, Maibach HI. Gender differences in skin aging and the changing profile of the sex hormones with age. J Steroids Horm Sci. 2012;3(2):109.	617 618
6.	Bucala R, Cerami A. Advanced Glycosylation: Chemistry, Biology, and Implications for Diabetes and Aging. In: August JT, Anders MW, Murad F, editors. Advances in Pharmacology [Internet]. Academic Press; 1992. p. 1–34. Available from: http://www.sciencedirect.com/science/article/pii/S1054358908609618	619 620 621
7.	Gkogkolou P, Böhm M. Advanced glycation end products. null. 2012 Jul 1;4(3):259–70.	622
8.	Hervé Pageon, Hélène Zucchi, Françoise Rousset, Vincent M. Monnier, Daniel Asselineau. Skin aging by glycation: lessons from the reconstructed skin model. Clinical Chemistry and Laboratory Medicine (CCLM). 2014;52(1):169–74.	623 624 625
9.	Lee DH, Oh JH, Chung JH. Glycosaminoglycan and proteoglycan in skin aging. Journal of Dermatological Science. 2016 Sep 1;83(3):174–81.	626 627
10.	Naylor EC, Watson REB, Sherratt MJ. Molecular aspects of skin ageing. Maturitas. 2011 Jul 1;69(3):249–56.	628
11.	Pageon H. Reaction of glycation and human skin: The effects on the skin and its components, reconstructed skin as a model. Pathologie Biologie. 2010 Jun 1;58(3):226–31.	629 630
12.	Pageon H, Técher MP, Asselineau D. Reconstructed skin modified by glycation of the dermal equivalent as a model for skin aging and its potential use to evaluate anti-glycation molecules. Experimental Gerontology. 2008 Jun 1;43(6):584–8.	631 632 633
13.	Bennett MF, Robinson MK, Baron ED, Cooper KD. Skin Immune Systems and Inflammation: Protector of the Skin or Promoter of Aging? Journal of Investigative Dermatology Symposium Proceedings. 2008 Apr 1;13(1):15–9.	634 635
14.	Janson D, Rietveld M, Willemze R, El Ghalbzouri A. Effects of serially passaged fibroblasts on dermal and epidermal morphogenesis in human skin equivalents. Biogerontology. 2013 Apr 1;14(2):131–40.	636 637
15.	Mansouri P, Chalangari R, Chalangari KM, Saffarian Z. Skin Aging and Immune System. In: Massoud A, Rezaei N, editors. Immunology of Aging [Internet]. Berlin, Heidelberg: Springer Berlin Heidelberg; 2014. p. 339–68. Available from: https://doi.org/10.1007/978-3-642-39495-9_25	638 639 640
16.	Varani J, Dame MK, Rittie L, Fligiel SEG, Kang S, Fisher GJ, Voorhees JJ. Decreased Collagen Production in Chronologically Aged Skin: Roles of Age-Dependent Alteration in Fibroblast Function and Defective Mechanical Stimulation. The American Journal of Pathology. 2006 Jun 1;168(6):1861–8.	641 642 643
17.	Tobin DJ. Introduction to skin aging. Journal of Tissue Viability. 2017 Feb 1;26(1):37–46.	644
18.	Berneburg M, Plettenberg H, Krutmann J. Photoaging of human skin. Photodermatology, Photoimmunology & Photomedicine. 2000 Dec 1;16(6):239–44.	645 646

Han A, Chien AL, Kang S. Photoaging. Dermatologic Clinics. 2014 Jul 1;32(3):291–9.

19.

20.	Helfrich YR. Sachs DL. V	oorhees II. Overview	of skin aging and r	photoaging, Derma	atology Nursing. 2008;20(3):177.

- 21. Bernstein EF, Brown DB, Schwartz MD, Kaidbey K, Ksenzenko SM. The Polyhydroxy Acid Gluconolactone Protects Against Ultraviolet Radiation in an In Vitro Model of Cutaneous Photoaging. Dermatologic Surgery. 2004 Feb 1;30(2):189–96.
- 22. Krutmann J. Ultraviolet A radiation-induced biological effects in human skin: relevance for photoaging and photodermatosis. Journal of Dermatological Science. 2000 Mar 1;23:S22–6.
- 23. Bernerd F, Asselineau D. Successive Alteration and Recovery of Epidermal Differentiation and Morphogenesis after Specific UVB-Damages in Skin Reconstructedin Vitro. Developmental Biology. 1997 Mar 15;183(2):123–38.
- 24. Kim EJ, Kim YK, Kim MK, Kim S, Kim JY, Lee DH, Chung JH. UV-induced inhibition of adipokine production in subcutaneous fat aggravates dermal matrix degradation in human skin. Scientific Reports. 2016 May 10;6(1):25616.
- 25. Quan T, He T, Kang S, Voorhees JJ, Fisher GJ. Solar Ultraviolet Irradiation Reduces Collagen in Photoaged Human Skin by Blocking Transforming Growth Factor-β Type II Receptor/Smad Signaling. The American Journal of Pathology. 2004 Sep 1;165(3):741–51.
- 26. Lee KE, Nho YH, Yun SK, Park SM, Kang S, Yeo H. Caviar Extract and Its Constituent DHA Inhibits UVB-Irradiated Skin Aging by Inducing Adiponectin Production. International Journal of Molecular Sciences. 2020 Jan;21(9):3383.
- 27. Kim WS, Park BS, Sung JH. Protective role of adipose-derived stem cells and their soluble factors in photoaging. 664
 Archives of Dermatological Research. 2009 Jun;301(5):329–36. 665
- 28. Watson REB, Griffiths CEM, Craven NM, Shuttleworth CA, Kielty CM. Fibrillin-Rich Microfibrils are Reduced in Photoaged Skin. Distribution at the Dermal–Epidermal Junction. Journal of Investigative Dermatology. 1999 May 1;112(5):782–7.
- 29. Bataillon M, Lelièvre D, Chapuis A, Thillou F, Autourde JB, Durand S, Boyera N, Rigaudeau AS, Besné I, Pellevoisin C. Characterization of a New Reconstructed Full Thickness Skin Model, T-Skin™, and its Application for Investigations of Anti-Aging Compounds. International Journal of Molecular Sciences. 2019 Jan;20(9):2240.
- 30. Charles-de-Sá L, Gontijo-de-Amorim N, Sbarbati A, Benati D, Bernardi P, Borojevic R, Carias RBV, Rigotti G. Photoaging Skin Therapy with PRP and ADSC: A Comparative Study. Colvin GA, editor. Stem Cells International. 2020 Jul 16;2020:2032359.
- 31. Smits JPH, Niehues H, Rikken G, Vlijmen-Willems IMJJ van, Zande GWHJF van de, Zeeuwen PLJM, Schalkwijk J, Bogaard EH van den. Immortalized N/TERT keratinocytes as an alternative cell source in 3D human epidermal models. Scientific Reports. 2017 Sep 19;7(1):11838.
- 32. Roger M, Fullard N, Costello L, Bradbury S, Markiewicz E, O'Reilly S, Darling N, Ritchie P, Määttä A, 678 Karakesisoglou I, Nelson G, Zglinicki T von, Dicolandrea T, Isfort R, Bascom C, Przyborski S. Bioengineering the 679

706

707

708

709

710

711

33.

70.

43.

44.

https://onlinelibrary.wiley.com/doi/abs/10.1111/joa.12942

	Misery L. Effects of the re-innervation of organotypic skin explants on the epidermis. Experimental Dermatology. 2011 Nov 29;21(2):156–8.	683 684
34.	El Ghalbzouri A, Commandeur S, Rietveld MH, Mulder AA, Willemze R. Replacement of animal-derived collagen matrix by human fibroblast-derived dermal matrix for human skin equivalent products. Biomaterials. 2009 Jan;30(1):71–8.	685 686 687
35.	van Drongelen V, Danso MO, Mulder A, Mieremet A, van Smeden J, Bouwstra JA, El Ghalbzouri A. Barrier Properties of an N/TERT-Based Human Skin Equivalent. Tissue Engineering Part A. 2014 May 13;20(21–22):3041–9.	688 689 690
36.	El Ghalbzouri A, Lamme E, Ponec M. Crucial role of fibroblasts in regulating epidermal morphogenesis. Cell and Tissue Research. 2002 Nov 1;310(2):189–99.	691 692
37.	El Ghalbzouri A, Jonkman MF, Dijkman R, Ponec M. Basement Membrane Reconstruction in Human Skin Equivalents Is Regulated by Fibroblasts and/or Exogenously Activated Keratinocytes. Journal of Investigative Dermatology. 2005 Jan 1;124(1):79–86.	693 694 695
38.	Mieremet A, Rietveld M, Absalah S, van Smeden J, Bouwstra JA, El Ghalbzouri A. Improved epidermal barrier formation in human skin models by chitosan modulated dermal matrices. PLOS ONE. 2017 Mar 23;12(3):e0174478.	696 697
39.	Taherzadeh O, Otto WR, Anand U, Nanchahal J, Anand P. Influence of human skin injury on regeneration of sensory neurons. Cell and Tissue Research. 2003 Jun 1;312(3):275–80.	698 699
40.	Black AF, Berthod F, L'heureux N, Germain L, Auger FA. In vitro reconstruction of a human capillary-like network in a tissue-engineered skin equivalent. The FASEB Journal. 1998 Oct 1;12(13):1331–40.	700 701
41.	Braziulis E, Diezi M, Biedermann T, Pontiggia L, Schmucki M, Hartmann-Fritsch F, Luginbühl J, Schiestl C, Meuli M, Reichmann E. Modified Plastic Compression of Collagen Hydrogels Provides an Ideal Matrix for Clinically Applicable Skin Substitutes. Tissue Engineering Part C: Methods. 2011 Dec 25;18(6):464–74.	702 703 704
42.	Thakoersing VS, Danso MO, Mulder A, Gooris G, Ghalbzouri AE, Bouwstra JA. Nature versus nurture: does	705

human skin maintain its stratum corneum lipid properties in vitro? Experimental Dermatology. 2012;21(11):865-

Thakoersing VS, Gooris GS, Mulder A, Rietveld M, El Ghalbzouri A, Bouwstra JA. Unraveling barrier properties

Batheja P, Song Y, Wertz P, Michniak-Kohn B. Effects of Growth Conditions on the Barrier Properties of a Human

of three different in-house human skin equivalents. Tissue Eng Part C Methods. 2012 Jan;18(1):1–11.

Skin Equivalent. Pharmaceutical Research. 2009 Jul 1;26(7):1689–700.

microanatomy of human skin. Journal of Anatomy [Internet]. [cited 2019 Feb 21];0(0). Available from:

Lebonvallet N, Boulais N, Le Gall C, Pereira U, Gauché D, Gobin E, Pers JO, Jeanmaire C, Danoux L, Pauly G,

58.

743

744

Fernandez TL, Van Lonkhuyzen DR, Dawson RA, Kimlin MG, Upton Z. Characterization of a Human Skin Equivalent Model to Study the Effects of Ultraviolet B Radiation on Keratinocytes. Tissue Engineering Part C: Methods. 2013 Nov 13;20(7):588-98. 714 Fleischmajer R, Utani A, MacDonald ED, Perlish JS, Pan TC, Chu ML, Nomizu M, Ninomiya Y, Yamada Y. 46. 715 Initiation of skin basement membrane formation at the epidermo-dermal interface involves assembly of laminins 716 through binding to cell membrane receptors. J Cell Sci. 1998 Jul 30;111(14):1929. 717 Marino D, Luginbühl J, Scola S, Meuli M, Reichmann E. Bioengineering Dermo-Epidermal Skin Grafts with Blood 718 and Lymphatic Capillaries. Science Translational Medicine. 2014 Jan 29;6(221):221ra14-221ra14. 719 48. Martins-Green M, Li QJ, Yao M. A new generation organ culture arising from cross-talk between multiple primary 720 human cell types. The FASEB Journal. 2004 Dec 9;19(2):222-4. 721 Kreimendahl F, Marquardt Y, Apel C, Bartneck M, Zwadlo-Klarwasser G, Hepp J, Jockenhoevel S, Baron JM. 722 Macrophages significantly enhance wound healing in a vascularized skin model. Journal of Biomedical Materials 723 Research Part A. 2019 Jun;107A:1340-50. 724 50. Bacqueville D, Mavon A. Comparative analysis of solar radiation-induced cellular damage between ex vivo 725 porcine skin organ culture and in vitro reconstructed human epidermis. International Journal of Cosmetic Science. 726 2009 Aug 1;31(4):293-302. 727 51. Zomer HD, Trentin AG. Skin wound healing in humans and mice: Challenges in translational research. Journal of 728 Dermatological Science. 2018 Apr 1;90(1):3–12. 729 52. Knight A. Systematic reviews of animal experiments demonstrate poor human clinical and toxicological utility. 730 Altern Lab Anim. 2007 Dec;35(6):641-59. 731 Bédard P, Gauvin S, Ferland K, Caneparo C, Pellerin È, Chabaud S, Bolduc S. Innovative Human Three-53. 732 Dimensional Tissue-Engineered Models as an Alternative to Animal Testing. Bioengineering (Basel). 2020 Sep 733 17;7(3):E115. 734 de Boo J, Hendriksen C. Reduction strategies in animal research: a review of scientific approaches at the intra-735 experimental, supra-experimental and extra-experimental levels. Altern Lab Anim. 2005 Aug;33(4):369-77. 736 Gangatirkar P, Paquet-Fifield S, Li A, Rossi R, Kaur P. Establishment of 3D organotypic cultures using human 55. 737 neonatal epidermal cells. Nature Protocols. 2007 Feb 8;2:178. 738 Breslin S, O'Driscoll L. Three-dimensional cell culture: the missing link in drug discovery. Drug Discovery Today. 56. 739 2013 Mar 1;18(5):240-9. 740 Shamir ER, Ewald AJ. Three-dimensional organotypic culture: experimental models of mammalian biology and 57. 741 disease. Nature Reviews Molecular Cell Biology. 2014 Oct 1;15(10):647-64. 742

Amelian A, Wasilewska K, Megias D, Winnicka K. Application of standard cell cultures and 3D in vitro tissue

models as an effective tool in drug design and development. Pharmacological Reports. 2017 Oct 1;69(5):861-70.

59.	Sanchez MM, Morgan JT. Generation of Self-assembled Vascularized Human Skin Equivalents. JoVE. 2021 Feb
	12;(168):e62125.

- 60. Sanchez MM, Orneles DN, Park BH, Morgan JT. Automated epidermal thickness quantification of in vitro human skin equivalents using optical coherence tomography. Biotechniques. 2022 May;72(5):194–200.
- 61. Chan RK, Zamora DO, Wrice NL, Baer DG, Renz EM, Christy RJ, Natesan S. Development of a Vascularized Skin Construct Using Adipose-Derived Stem Cells from Debrided Burned Skin. Meisel R, editor. Stem Cells International. 2012 Jul 5;2012:841203.
- 62. Bellas E, Seiberg M, Garlick J, Kaplan DL. In vitro 3D Full-Thickness Skin-Equivalent Tissue Model Using Silk and Collagen Biomaterials. Macromolecular Bioscience. 2012 Dec 1;12(12):1627–36.
- 63. Kober J, Gugerell A, Schmid M, Kamolz LP, Keck M. Generation of a Fibrin Based Three-Layered Skin Substitute. Kasper C, editor. BioMed Research International. 2015 Jul 7;2015:170427.
- 64. Huber B, Link A, Linke K, Gehrke SA, Winnefeld M, Kluger PJ. Integration of Mature Adipocytes to Build-Up a Functional Three-Layered Full-Skin Equivalent. Tissue Engineering Part C: Methods. 2016 Jun 22;22(8):756–64.
- 65. Kon A, Takeda H, Ito N, Hanada K, Takagaki K. Tissue-specific downregulation of type VII collagen gene (COL7A1) transcription in cultured epidermal keratinocytes by ultraviolet A radiation (UVA) and UVA-inducible cytokines, with special reference to cutaneous photoaging. Journal of Dermatological Science Supplement. 2005 Dec 1;1(2):S29–35.
- 66. Son WC, Yun JW, Kim BH. Adipose-derived mesenchymal stem cells reduce MMP-1 expression in UV-irradiated human dermal fibroblasts: therapeutic potential in skin wrinkling. null. 2015 Jun 3;79(6):919–25.
- 67. Qin H, Zhang G, Zhang L. GSK126 (EZH2 inhibitor) interferes with ultraviolet A radiation-induced photoaging of human skin fibroblast cells. Exp Ther Med. 2018 Apr 1;15(4):3439–48.
- 68. Dickson MA, Hahn WC, Ino Y, Ronfard V, Wu JY, Weinberg RA, Louis DN, Li FP, Rheinwald JG. Human keratinocytes that express hTERT and also bypass a p16(INK4a)-enforced mechanism that limits life span become immortal yet retain normal growth and differentiation characteristics. Mol Cell Biol. 2000 Feb;20(4):1436–47.
- 69. Ades EW, Candal FJ, Swerlick RA, George VG, Summers S, Bosse DC, Lawley TJ. HMEC-1: establishment of an immortalized human microvascular endothelial cell line. Journal of Investigative Dermatology. 1992;99(6):683–90.
- 70. Wolbank S, Stadler G, Peterbauer A, Gillich A, Karbiener M, Streubel B, Wieser M, Katinger H, van Griensven M, Redl H, Gabriel C, Grillari J, Grillari-Voglauer R. Telomerase Immortalized Human Amnion- and Adipose-Derived Mesenchymal Stem Cells: Maintenance of Differentiation and Immunomodulatory Characteristics. Tissue Engineering Part A. 2009 Jul 1;15(7):1843–54.
- 71. Morgan JT, Wood JA, Walker NJ, Raghunathan VK, Borjesson DL, Murphy CJ, Russell P. Human Trabecular Meshwork Cells Exhibit Several Characteristics of, but Are Distinct from, Adipose-Derived Mesenchymal Stem Cells. Journal of Ocular Pharmacology and Therapeutics. 2014 Jan 23;30(2–3):254–66.

- 72. Yu G, Floyd ZE, Wu X, Hebert T, Halvorsen YDC, Buehrer BM, Gimble JM. Adipogenic Differentiation of Adipose-Derived Stem Cells. In: Gimble JM, Bunnell BA, editors. Adipose-Derived Stem Cells: Methods and Protocols [Internet]. Totowa, NJ: Humana Press; 2011. p. 193–200. Available from: https://doi.org/10.1007/978-1-61737-960-4_14
- 73. Zhang Z, Michniak-Kohn BB. Tissue Engineered Human Skin Equivalents. Pharmaceutics. 2012;4(1).
- 74. Tajima S, Pinnell SR. Ascorbic acid preferentially enhances type I and III collagen gene transcription in human skin fibroblasts. Journal of Dermatological Science. 1996 Mar 1;11(3):250–3.
- 75. Murad S, Tajima S, Johnson GR, Sivarajah A, Pinnell SR. Collagen Synthesis in Cultured Human Skin Fibroblasts: Effect of Ascorbic Acid and Its Analogs. Journal of Investigative Dermatology. 1983 Aug 1;81(2):158–62.
- 76. Villacorta L, Azzi A, Zingg JM. Regulatory role of vitamins E and C on extracellular matrix components of the vascular system. Molecular Aspects of Medicine. 2007 Oct 1;28(5):507–37.
- 77. Ashino H, Shimamura M, Nakajima H, Dombou M, Kawanaka S, Oikawa T, Iwaguchi T, Kawashima S. Novel Function of Ascorbic Acid as an Angiostatic Factor. Angiogenesis. 2003 Dec 1;6(4):259–69.
- 78. Ponec M, Weerheim A, Kempenaar J, Mulder A, Gooris GS, Bouwstra J, Mieke Mommaas A. The Formation of Competent Barrier Lipids in Reconstructed Human Epidermis Requires the Presence of Vitamin C. Journal of Investigative Dermatology. 1997 Sep 1;109(3):348–55.
- 79. Morgan JT, Shirazi J, Comber EM, Eschenburg C, Gleghorn JP. Fabrication of centimeter-scale and geometrically arbitrary vascular networks using in vitro self-assembly. Biomaterials. 2019 Jan 1;189:37–47.
- 80. Bornstein MB. Reconstituted rat-tail collagen used as substrate for tissue cultures on coverslips in Maximow slides and roller tubes. Laboratory Investigation. 1958;7(2):134–7.
- 81. Cross VL, Zheng Y, Won Choi N, Verbridge SS, Sutermaster BA, Bonassar LJ, Fischbach C, Stroock AD. Dense type I collagen matrices that support cellular remodeling and microfabrication for studies of tumor angiogenesis and vasculogenesis in vitro. Biomaterials. 2010 Nov 1;31(33):8596–607.
- 82. Rajan N, Habermehl J, Coté MF, Doillon CJ, Mantovani D. Preparation of ready-to-use, storable and reconstituted type I collagen from rat tail tendon for tissue engineering applications. Nature Protocols. 2007 Jan 18;1:2753.
- 83. Clément MV, Ramalingam J, Long LH, Halliwell B. The In Vitro Cytotoxicity of Ascorbate Depends on the Culture Medium Used to Perform the Assay and Involves Hydrogen Peroxide. Antioxidants & Redox Signaling. 2001 Feb 1;3(1):157–63.
- 84. Duval C, Schmidt R, Regnier M, Facy V, Asselineau D, Bernerd F. The use of reconstructed human skin to evaluate UV-induced modifications and sunscreen efficacy. Experimental Dermatology. 2003 Oct 1;12(s2):64–70.
- 85. Tanaka K, Asamitsu K, Uranishi H, Iddamalgoda A, Ito K, Kojima H, Okamoto T. Protecting skin photoaging by NF-kappaB inhibitor. Current Drug Metabolism. 2010 Jun 1;11(5):431–5.

840

86.	Shirazi J, Morgan JT, Comber EM, Gleghorn JP. Generation and morphological quantification of large scale, three-dimensional, self-assembled vascular networks. MethodsX. 2019;6:1907–18.	81 81
87.	Kovesi P. Phase preserving denoising of images. In: signal. Perth, WA; 1999. p. 212–7.	81
88.	Kovesi P. Phase Preserving Tone Mapping of Non-Photographic High Dynamic Range Images. In: Digital Image Computing: Techniques and Applications DICTA 2012. 2012.	81: 81:
89.	Jerman T. Jerman Enhancement Filter [Internet]. 2021. Available from: Tim Jerman (2021). Jerman Enhancement Filter (https://github.com/timjerman/JermanEnhancementFilter), GitHub. Retrieved August 12, 2021.	81 81
90.	T. Jerman, F. Pernuš, B. Likar, Ž. Špiclin. Enhancement of Vascular Structures in 3D and 2D Angiographic Images. IEEE Transactions on Medical Imaging. 2016 Sep;35(9):2107–18.	81°
91.	Tim Jerman, Franjo Pernuš, Boštjan Likar, Žiga Špiclin. Beyond Frangi: an improved multiscale vesselness filter. In 2015. Available from: https://doi.org/10.1117/12.2081147	81°
92.	Van Uitert R, Bitter I. Subvoxel precise skeletons of volumetric data based on fast marching methods. Medical Physics. 2007 Feb 1;34(2):627–38.	82 82
93.	Sethian JA. A fast marching level set method for monotonically advancing fronts. Proc Natl Acad Sci U S A. 1996 Feb 20;93(4):1591–5.	82 82
94.	Sethian JA. Fast Marching Methods. SIAM Rev. 1999 Jan 1;41(2):199–235.	82
95.	Wang Y, Oh CM, Oliveira MC, Islam MS, Ortega A, Park BH. GPU accelerated real-time multi-functional spectral-domain optical coherence tomography system at 1300 nm. Opt Express. 2012 Jul 2;20(14):14797–813.	82°
96.	Kim EJ, Kim YK, Kim JE, Kim S, Kim MK, Park CH, Chung JH. UV Modulation of Subcutaneous Fat Metabolism. Journal of Investigative Dermatology. 2011 Aug 1;131(8):1720–6.	82°
97.	Chung JH, Yano K, Lee MK, Youn CS, Seo JY, Kim KH, Cho KH, Eun HC, Detmar M. Differential Effects of Photoaging vs Intrinsic Aging on the Vascularization of Human Skin. Archives of Dermatology. 2002 Nov 1;138(11):1437–42.	83 83 83
98.	Rittié L, Fisher GJ. Natural and Sun-Induced Aging of Human Skin. Cold Spring Harb Perspect Med. 2015 Jan 1;5(1):a015370.	83
99.	Dos Santos M, Metral E, Boher A, Rousselle P, Thepot A, Damour O. In vitro 3-D model based on extending time of culture for studying chronological epidermis aging. Matrix Biology. 2015 Sep 1;47:85–97.	83
100.	Diekmann J, Alili L, Scholz O, Giesen M, Holtkötter O, Brenneisen P. A three-dimensional skin equivalent reflecting some aspects of in vivo aged skin. Experimental Dermatology. 2016 Jan 1;25(1):56–61.	83

101. Weinmüllner R, Zbiral B, Becirovic A, Stelzer EM, Nagelreiter F, Schosserer M, Lämmermann I, Liendl L, Lang M,

Terlecki-Zaniewicz L, Andriotis O, Mildner M, Golabi B, Waidhofer-Söllner P, Schedle K, Emsenhuber G, Thurner

869

870

PJ, Tschachler E, Gruber F, Grillari J. Organotypic human skin culture models constructed with senescent fibroblasts show hallmarks of skin aging, npj Aging and Mechanisms of Disease. 2020 Mar 6;6(1):4. 102. Youn SW, Kim DS, Cho HJ, Jeon SE, Bae IH, Yoon HJ, Park KC. Cellular senescence induced loss of stem cell 843 proportion in the skin in vitro. Journal of Dermatological Science. 2004 Aug 1;35(2):113-23. 844 103. Adamus J, Aho S, Meldrum H, Bosko C, Lee JM. p16INK4A influences the aging phenotype in the living skin 845 equivalent. J Invest Dermatol. 2013/11/11 ed. 2014 Apr;134(4):1131-3. 846 104. Ressler S, Bartkova J, Niederegger H, Bartek J, Scharffetter-Kochanek K, Jansen-Dürr P, Wlaschek M. p16INK4A 847 is a robust in vivo biomarker of cellular aging in human skin. Aging Cell. 2006 Oct 1;5(5):379-89. 848 105. Hervé Pageon, Hilaire Bakala, Vincent M Monnier, Daniel Asselineau. Collagen glycation triggers the formation 849 of aged skin in vitro. European Journal of Dermatology. 2007 Jan 1;17(1):12-20. 850 106. Sok J, Pineau N, Dalko-Csiba M, Breton L, Bernerd F. Improvement of the dermal epidermal junction in human 851 reconstructed skin by a new c-xylopyranoside derivative. European Journal of Dermatology. 2008;18(3):297–302. 852 107. Claire DELOCHE, Anne Marie MINONDO, Bruno A. BERNARD, Françoise BERNERD, Fabien SALAS, Julien 853 GARNIER, Emmanuelle TANCRÈDE. Effect of C-xyloside on morphogenesis of the dermal epidermal junction in 854 aged female skin. An unltrastuctural pilot study. European Journal of Dermatology. 2011 May 1;21(2):191–6. 855 108. Vassal-Stermann E, Duranton A, Black AF, Azadiguian G, Demaude J, Lortat-Jacob H, Breton L, Vivès RR. A New 856 C-Xyloside Induces Modifications of GAG Expression, Structure and Functional Properties. PLOS ONE. 2012 Oct 857 26;7(10):e47933. 858 109. ASCHER B, COLEMAN S, ALSTER T, BAUER U, BURGESS C, BUTTERWICK K, DONOFRIO L, ENGELHARD 859 P, GOLDMAN MP, KATZ P, VLEGGAAR D. Full Scope of Effect of Facial Lipoatrophy: A Framework of Disease 860 Understanding. Dermatologic Surgery. 2006 Aug 1;32(8):1058-69. 861 110. Saely CH, Geiger K, Drexel H. Brown versus white adipose tissue: a mini-review. Gerontology. 2012;58(1):15–23. 862 111. Fiorenza CG, Chou SH, Mantzoros CS. Lipodystrophy: pathophysiology and advances in treatment. Nature 863 Reviews Endocrinology. 2011 Mar 1;7(3):137-50. 864 112. Reitman ML, Arioglu E, Gavrilova O, Taylor SI. Lipoatrophy Revisited. Trends in Endocrinology & Metabolism. 865 2000 Dec 1;11(10):410-6. 866 113. Hammel JH, Bellas E. Endothelial cell crosstalk improves browning but hinders white adipocyte maturation in 867

114. Kang JH, Gimble JM, Kaplan DL. In Vitro 3D Model for Human Vascularized Adipose Tissue. Tissue Engineering

3D engineered adipose tissue. Integrative Biology. 2020 Mar 26;12(4):81–9.

Part A. 2009 Feb 6;15(8):2227-36.

115.	Mauney JR, Nguyen T, Gillen K, Kirker-Head C, Gimble JM, Kaplan DL. Engineering adipose-like tissue in vitro and in vivo utilizing human bone marrow and adipose-derived mesenchymal stem cells with silk fibroin 3D scaffolds. Biomaterials. 2007 Dec 1;28(35):5280–90.
116.	Trottier V, Marceau-Fortier G, Germain L, Vincent C, Fradette J. IFATS Collection: Using Human Adipose-Derived Stem/Stromal Cells for the Production of New Skin Substitutes. STEM CELLS. 2008 Oct 1;26(10):2713–23.
117.	Smith LE, Bonesi M, Smallwood R, Matcher SJ, MacNeil S. Using swept-source optical coherence tomography to monitor the formation of neo-epidermis in tissue-engineered skin. Journal of Tissue Engineering and Regenerative Medicine. 2010 Dec 1;4(8):652–8.
118.	Gambichler T, Matip R, Moussa G, Altmeyer P, Hoffmann K. In vivo data of epidermal thickness evaluated by optical coherence tomography: Effects of age, gender, skin type, and anatomic site. Journal of Dermatological Science. 2006 Dec 1;44(3):145–52.

- 119. Battie C, Jitsukawa S, Bernerd F, Del Bino S, Marionnet C, Verschoore M. New insights in photoaging, UVA induced damage and skin types. Experimental Dermatology. 2014 Oct 1;23(s1):7–12.
- 120. Agar NS, Halliday GM, Barnetson RStC, Ananthaswamy HN, Wheeler M, Jones AM. The basal layer in human squamous tumors harbors more UVA than UVB fingerprint mutations: A role for UVA in human skin carcinogenesis. Proc Natl Acad Sci U S A. 2004 Apr 6;101(14):4954.
- 121. Braverman IM. The Cutaneous Microcirculation. Journal of Investigative Dermatology Symposium Proceedings. 2000 Dec 1;5(1):3–9.
- 122. Kim BS, Gao G, Kim JY, Cho DW. 3D Cell Printing of Perfusable Vascularized Human Skin Equivalent Composed of Epidermis, Dermis, and Hypodermis for Better Structural Recapitulation of Native Skin. Advanced Healthcare Materials. 2019 Apr 1;8(7):1801019.
- 123. Mertsching H, Walles T, Hofmann M, Schanz J, Knapp WH. Engineering of a vascularized scaffold for artificial tissue and organ generation. Biomaterials. 2005 Nov 1;26(33):6610–7.
- 124. Men SJ, Chen CL, Wei W, Lai TY, Song SZ, Wang RK. Repeatability of vessel density measurement in human skin by OCT-based microangiography. Skin Res Technol. 2017/05/17 ed. 2017 Nov;23(4):607–12.
- 125. Cao Y, Wang H, Wang Q, Han X, Zeng W. Three-dimensional volume fluorescence-imaging of vascular plasticity in adipose tissues. Molecular Metabolism. 2018 Aug 1;14:71–81.
- 126. Huber B, Volz AC, Kluger PJ. Understanding the effects of mature adipocytes and endothelial cells on fatty acid metabolism and vascular tone in physiological fatty tissue for vascularized adipose tissue engineering. Cell and Tissue Research. 2015 Nov 1;362(2):269–79.
- 127. Kligman AM. Perspectives and Problems in Cutaneous Gerontology. Journal of Investigative Dermatology. 1979 Jul 1;73(1):39–46.

933

128.	Lovett M, Lee K, Edwards A, Kaplan DL. Vascularization Strategies for Tissue Engineering. Tissue Engineering Part B: Reviews. 2009 Sep 1;15(3):353–70.	903 904
129.	Kim MS, Kim YK, Eun HC, Cho KH, Chung JH. All-Trans Retinoic Acid Antagonizes UV-Induced VEGF Production and Angiogenesis via the Inhibition of ERK Activation in Human Skin Keratinocytes. Journal of Investigative Dermatology. 2006 Dec 1;126(12):2697–706.	905 906 907
130.	Braverman IM, Yen A. ULTRASTRUCTURE OF THE CAPILLARY LOOPS IN THE DERMAL PAPILLAE OF PSORIASIS. Journal of Investigative Dermatology. 1977 Jan 1;68(1):53–60.	908 909
131.	Arai Y, Takayama M, Abe Y, Hirose N. Adipokines and Aging. Journal of Atherosclerosis and Thrombosis. 2011;advpub:1105060376–1105060376.	910 911
132.	Kadowaki T, Yamauchi T. Adiponectin and Adiponectin Receptors. Endocrine Reviews. 2005 May 1;26(3):439–51.	912
133.	Schneider LA, Raizner K, Wlaschek M, Brenneisen P, Gethöffer K, Scharffetter-Kochanek K. UVA-1 exposure in vivo leads to an IL-6 surge within the skin. Experimental Dermatology. 2017 Sep 1;26(9):830–2.	913 914
134.	Wlaschek M, Bolsen K, Herrmann G, Schwarz A, Wilmroth F, Heinrich PC, Goerz G, Scharffetter-Kochanek K. UVA-Induced Autocrine Stimulation of Fibroblast-Derived-Collagenase by IL-6: A Possible Mechanism in Dermal Photodamage? Journal of Investigative Dermatology. 1993 Aug 1;101(2):164–8.	915 916 917
135.	Vielhaber G, Grether-Beck S, Koch O, Johncock W, Krutmann J. Sunscreens with an absorption maximum of \geq 360 nm provide optimal protection against UVA1-induced expression of matrix metalloproteinase-1, interleukin-1, and interleukin-6 in human dermal fibroblasts. Photochemical & Photobiological Sciences. 2006;5(3):275–82.	918 919 920
136.	Jor JWY, Parker MD, Taberner AJ, Nash MP, Nielsen PMF. Computational and experimental characterization of skin mechanics: identifying current challenges and future directions. Wiley Interdiscip Rev Syst Biol Med. 2013;5(5):539–56.	921 922 923
137.	Shuster S, Black MM, McVitie E. The influence of age and sex on skin thickness, skin collagen and density. British Journal of Dermatology. 1975 Dec 1;93(6):639–43.	924 925
138.	Grinnell F, Lamke CR. Reorganization of hydrated collagen lattices by human skin fibroblasts. Journal of Cell Science. 1984 Mar 1;66(1):51–63.	926 927
139.	Ridge MD, Wright V. The directional effects of skin. A bio-engineering study of skin with particular reference to Langer's lines. J Invest Dermatol. 1966 Apr;46(4):341–6.	928 929
140.	Ahmed A, Joshi IM, Mansouri M, Ahamed NNN, Hsu MC, Gaborski TR, Abhyankar VV. Engineering fiber anisotropy within natural collagen hydrogels. Am J Physiol Cell Physiol. 2021 Jun 1;320(6):C1112–24.	930 931

141. Dewle A, Pathak N, Rakshasmare P, Srivastava A. Multifarious Fabrication Approaches of Producing Aligned

Collagen Scaffolds for Tissue Engineering Applications. ACS Biomater Sci Eng. 2020 Feb 10;6(2):779–97.

142.	Angel P, Szabowski A, Schorpp-Kistner M. Function and regulation of AP-1 subunits in skin physiology and	934
	pathology. Oncogene. 2001 Apr 1;20(19):2413–23.	935
143.	Zghoul N, Fuchs R, Lehr CM, Schaefer UF. Reconstructed skin equivalents for assessing percutaneous drug	936
	absorption from pharmaceutical formulations. ALTEX-Alternatives to animal experimentation. 2001;18(2):103-6.	937

144. Xie Y, Rizzi SC, Dawson R, Lynam E, Richards S, Leavesley DI, Upton Z. Development of a three-dimensional human skin equivalent wound model for investigating novel wound healing therapies. Tissue Engineering Part C: Methods. 2010;16(5):1111–23.

941

938

939